Comparative study between Proportional Integral and Neural Networks Controllers of a Shunt Active Power Filter Powered by a Photovoltaic System

Abdelkader Morsli[1,2], Wahiba Menasri[2], Amel Abbadi[1], Fethia Hamidia[1], Abdelhalim Tlemçani[1], Faouzi Didi[2], Moustafa Sahnoune Chaouche[2]

[1] Research Laboratory on Electrical Engineering and Automatic (LREA), University of Medea, 26000, Algeria

[2] Renewable Energies and Materials Laboratory (LERM), University of Medea, Medea, 26000, Algeria

(Corresponding Author): *E-mail: Morsli.aek2016@gmail.com

Received: 22-02-2023 **Accepted:** 29-04-2023 **Published:** 06-05-2023

Abstract

The objective of this paper is the study of the implementation of compensation algorithms using shunt active power filter with voltage structure, for the mitigation of harmonic currents generated by nonlinear loads in distorted electrical networks. This work presents an approach to reduce the harmonic distortion rate (THD) of the source current and other approaches to improve the power factor by a parallel active power filter. For this, I will present a structure of inverter of two levels on the one hand, and the different control techniques between classical and intelligent on the other hand. To do this, a miniature prototype simulation of a control of a SAPF by (PI) and (ANN) controllers powered by photovoltaic source has been established. These controllers are used with instantaneous active and reactive powers method (PQ). The simulation results allow us to understand the importance of increasing the level of the inverter and the control strategy used for the improvement of the THD and the power factor at the same time.

Keywords: Active Filters; Artificial Neural Networks; Maximum Power Point Trackers; Photovoltaic Systems; Proportional Control; Reactive Power Control.

Tob Regul Sci. ™ 2023;9(1): 1698-1713
DOI: doi.org/10.18001/TRS.9.1.116

Introduction

In view of the quality of electrical energy which has become the source of concern for users and their electrical power sources, because of the major non-linear electrical loads used by customers [1].

Currently, active power filters are widely used for reactive energy compensation in the electrical grid. These filters replace passive filters that are inconvenient.

The Shunt Active Power Filters are used as current sources in order to minimize harmonics as much as possible and by injecting filter currents to compensate reactive power [1, 2].

The power source of an inverter is provided by a DC-Link bus capacitor. This connection represents a SAPF by ensuring high switching frequencies passing through a coupling inductor and connected to the three-phase system in a common connection point (CCP) [3].

Recently, the intelligent controllers were used to replace the conventional proportional integral (PI) that is used [4].

The disadvantages of traditional solutions that no longer meet the requirements of modern power grids and the emergence of semiconductor-based switches, have led researchers and electric power producers to propose a new structure of a modern and efficient solution called shunt Active Power Filter (SAPF) [5].

For three decades, the principle of the Active Power Filter has been known. But its possibility of realization was limited according to the improvement of the devices possessing switching speed [6, 7].

In this paper, the technique of the ANN command is proposed for the control of the SAPF. To enhance the performance of the p-q method, a self-adjusting filter is suggested and provides better identification. The simulation is performed under the MATLAB/ Simulink environment. The results of the simulation obtained demonstrate the improvement of the energy quality and prevent its reliability of the ANN control compared to the conventional PI regulator. We have exploited photovoltaic solar energy as a free source to power the two-level voltage inverter instead of DC link. This source has many advantages such as cleanliness, inexhaustible, less maintenance by human beings and availability in rural areas. The command of the dc-dc boost converter is also made to optimize the energy produced by the photovoltaic panels; it is the control by (P & O) which is usual used in this field.

Thus, the aim of this work is to improve the THD (i.e. the THD of the source current becomes less than five percent and increase the power factor in such a way that it is close to unity).

2. The Shunt Active Power Filter system

In the common connection point (CCP), we connect a Shunt Active Power Filter between the three phase source and the nonlinear load which is the main source of harmonics in the power lines. To have a good resolution, we use a correction filter (L_F, R_F). [8, 9, 10].

Figure 1 shows the schematic diagram of the SAPF.

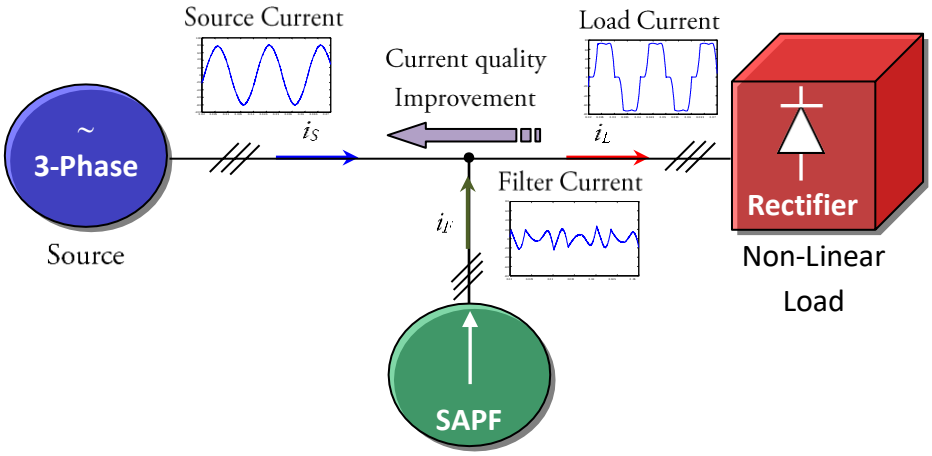

Figure 1. The schematic diagram of the SAPF

Figure 2 shows the detail of the diagram shown in Figure 1. The source is a low-voltage balanced three-phase power system that supplies the non-linear load (rectifier) via lines that carry inductors L_{Sabc} and resistors R_{Sabc} with sinusoidal currents i_{Sabc}. In this role, the rectifier injects significant harmonic currents into the power grid that affect the power system and deform the i_{Labc} waveforms. For this purpose, we have injected at the common connection point a static voltage inverter which delivers equal counter-harmonic currents i_{Fabc} of the harmonics of the non-linear load but in phase opposition.

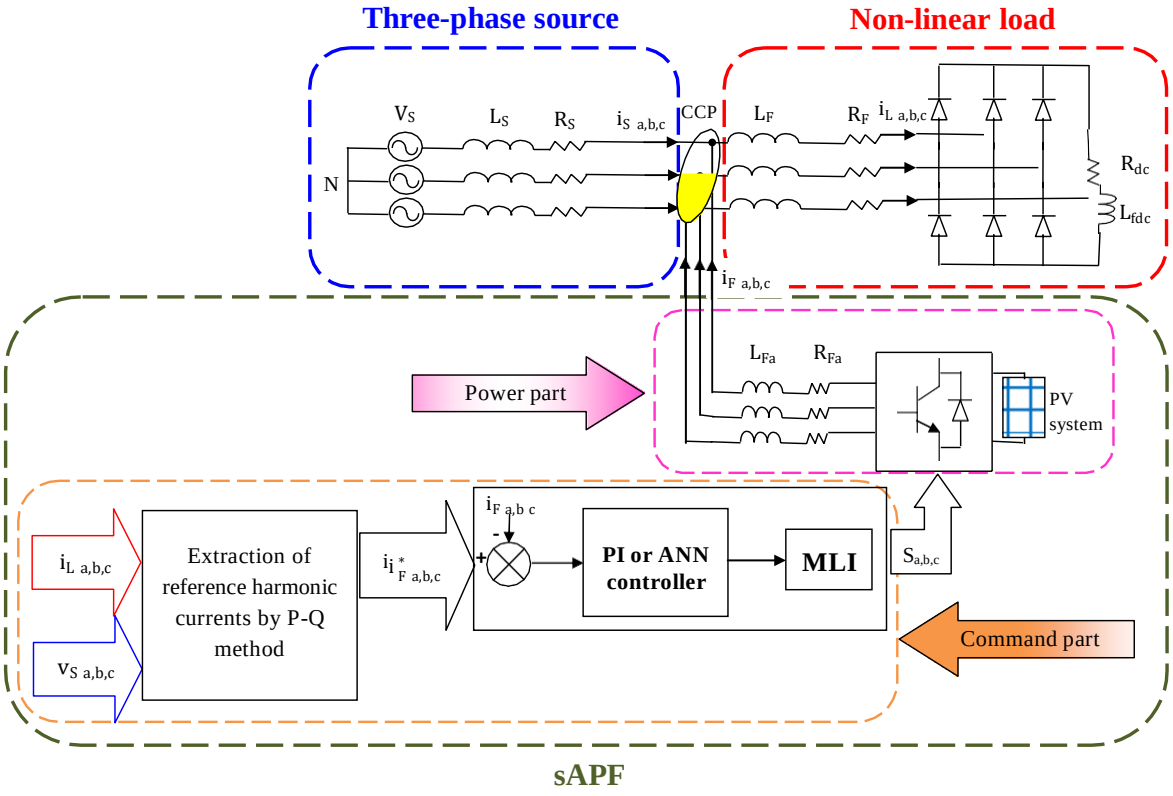

Figure 2. Model of the Shunt Active Power filtering system used

3. The photovoltaic solar system

In the simulation of the MPPT technique, the MATLAB/Simulink was used because of the possibility of simulating mixed systems (continuous and discrete) the continuous system is used for the simulation of the different analog parts (Solar panel and DC-DC converter), the discrete system is used to simulate algorithmic tracking method by (P&O) (Figure3) [11]. Mathematicians have modeled each organ of the photovoltaic system, the PV generator, the DC-DC converter and the MPPT controller as we will see in sections A, B and C.

3.1. The Photovoltaic solar panel

Figure 4 shows the electrical circuit of single diode PV module.

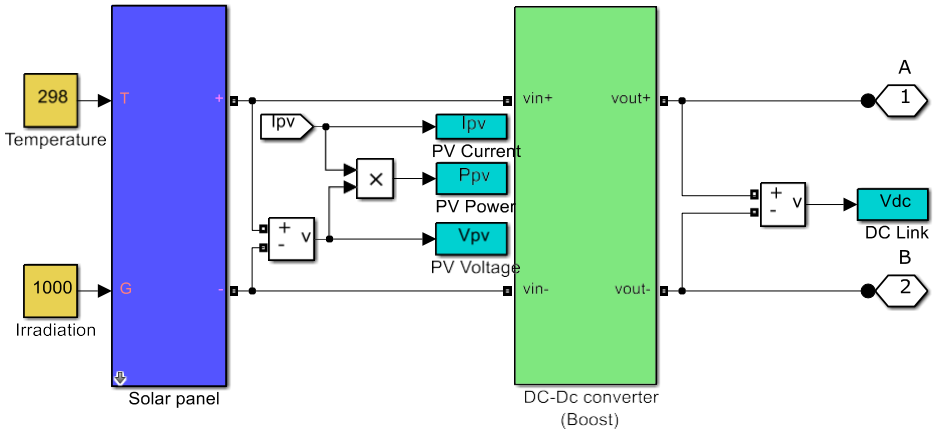

Figure 3. Model of the proposed photovoltaic system

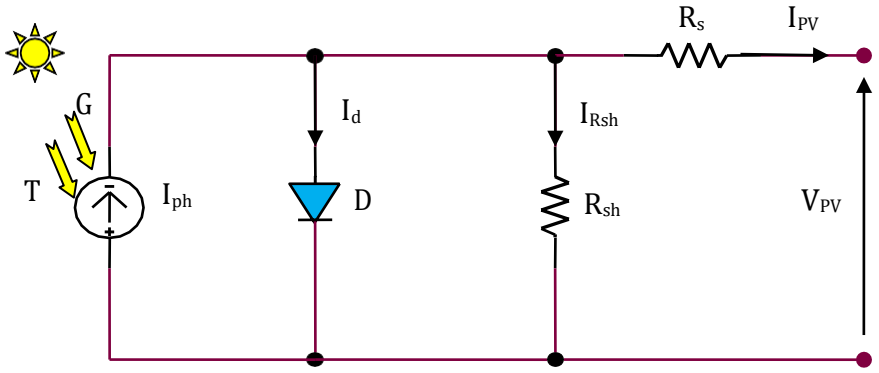

Figure 4. Electrical circuit of a PV solar panel

The equivalent electric circuit of a real photovoltaic module with a single diode delivers an electric current which can be written as follows [12]:

$$I_{PV} = I_{ph} - I_0 \left[e^{\frac{V_{PV}+I_{PV}\cdot R_S}{a\cdot V_T}} - 1 \right] - \frac{V_{PV}+I_{PV}\cdot R_S}{R_{Sh}} \quad (1)$$

with,

$$V_T = \frac{N_S \cdot K \cdot T}{q} \quad (2)$$

The photocurrent is given by:

$$I_{ph} = \left(I_{ph,STC} + K_I \cdot \Delta T\right) \cdot \frac{G}{G_{STC}} \quad (3)$$

And the reverse saturation current:

$$I_0 = \frac{I_{ph,STC} + K_I \cdot \Delta T}{e^{\frac{V_{OC,STC} + KV \cdot \Delta T}{a \cdot V_T}} - 1} \quad (4)$$

For large arrays composed of $Nss \cdot N_{pp}$ modules the previous equations of one and two become:

$$I_{PV} = I_{ph} \cdot N_{pp} - I_0 \cdot N_{pp} \left\{ e^{\frac{V_{PV} + I_{PV} \cdot R_S \cdot \left(\frac{N_{ss}}{N_{pp}}\right)}{a \cdot V_T}} - 1 \right\} - \frac{V_{PV} + I_{PV} \cdot R_S \cdot \left(\frac{N_{ss}}{N_{pp}}\right)}{R_{Sh} \cdot \left(\frac{N_{ss}}{N_{pp}}\right)} \quad (5)$$

with,

I_{pv} : output current of photovoltaic module,
V_{pv} : output voltage of photovoltaic module,
I_{ph} : photocurrent,
I_0 : reverse saturation current of diode,
a : diode ideality factor,
k : Boltzmann constant $k = 1.38 \times 10^{-23}\, J/°K$,
T : p-n junction temperature,
q : electron charge $q = 1.6 \times 10^{-19} C$,
K_i : short-circuit current/temperature coefficient,
K_v : open-circuit voltage/temperature coefficient,
G : actual sun irradiation,
G_{STC} : nominal sun irradiation (1000W/m^2) ,
ΔT : difference between Actual temperature and nominal temperature (25°C).

The PV modules are of type BP-MSX120, their characteristics are given on the Table 1.

Table I. Datasheet parameters of the PV module

BP SOLAR MSX 120	
Maximum Power Point (P_{max})	120 W
Voltage at P_{max} (V_{mp})	33.7 V
Current at P_{max} (I_{mp})	3.56 A
Open-circuit voltage (V_{oc})	42.1 V
Short-circuit current (I_{sc})	3.87 A
Series resistance (R_s)	0.473 Ω
Shunt resistance (R_{sh})	1367 Ω
Ideality factor (n)	1.3977
Temperature coefficient of I_{sc} (k_i)	(0.065±0.015) %/°C
Temperature coefficient of V_{oc} (k_v)	-(80±10) mV/°C

Temperature coefficient of power	-(0.5±0.05) %/°C
NOCT	47±2 °C
Number of cells connected in series (n_{cs})	72

The $I_{PV}-V_{PV}$ and $P_{PV}-V_{PV}$ curves of a typical photovoltaic module are shown in f Figure 5:

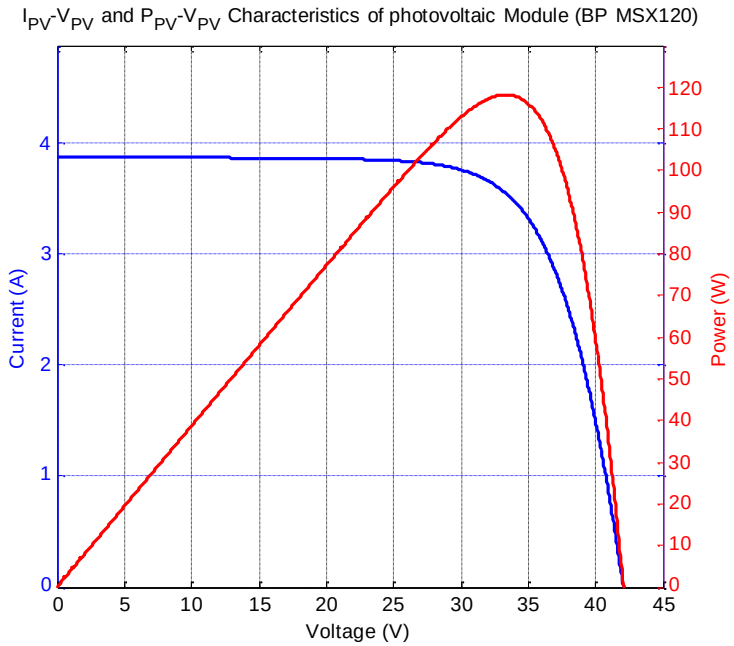

Figure 5. Electrical characteristics curves of the current and the power in function of the voltage of a photovoltaic module type BP MSX120

3.2. The dc-dc converter (boost)

Figure 6 shows the used DC-DC boost converter with MPPT controller by perturb and observe (P&O) algorithm.

The following equations are obtained from Fig. 3 when the switch is open. The peride T ∈ [DT_s, T_s]:

$$i_{c,in}(t) = C_{in}\frac{dv_i(t)}{dt} = i(t) - i_L(t) \quad (6)$$

$$i_{c,out}(t) = C_{out}\frac{dv_o(t)}{dt} = i_L(t) - i_o(t) \quad (7)$$

$$v_1(t) = L\frac{di_L(t)}{dt} = v_i(t) - v_o(t) \quad (8)$$

The conversion ratio M (D) of an ideal boost converter is given on the expression (9):

$$M(D) = \frac{v_o}{v_i} = M(D) = \frac{v_o}{v_i} = \frac{1}{D'} = \frac{1}{1-D} \quad (9)$$

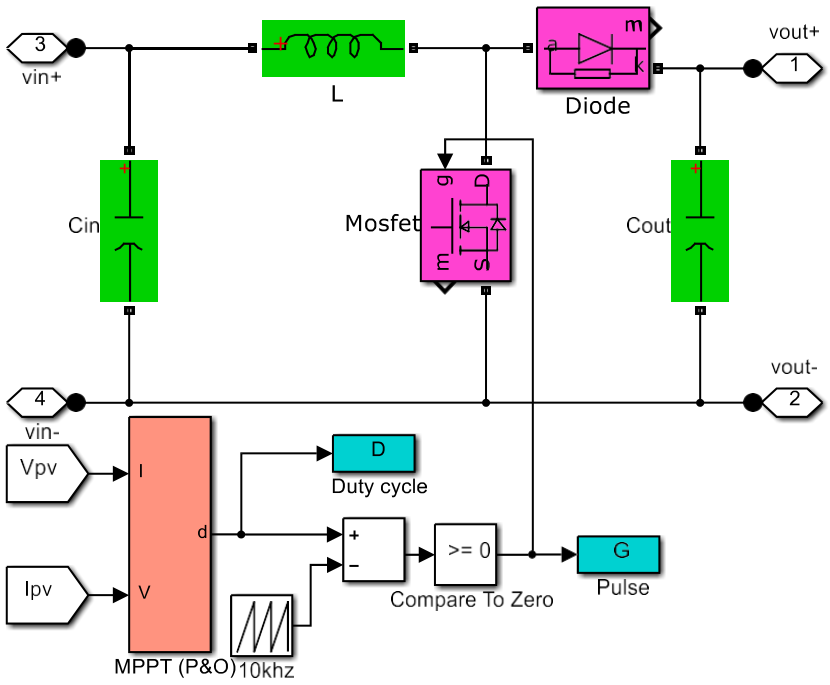

Figure 6. Principal scheme of DC-DC boost converter

The conversion ratio M (D) of an ideal boost converter is given on the expression (9):

$$M(D) = \frac{v_o}{v_i} = M(D) = \frac{v_o}{v_i} = \frac{1}{D'} = \frac{1}{1-D} \qquad (9)$$

3.3. The MPPT controller with Prturb and Observe (P&O)

This transistor controlled by the (P& O) algorithm aims to tracking the maximum power point MPPT. The latter is then controlled using a MPPT controller with the (P&O) algorithm, as shown in Figure 7.

4. Shunt Active Power Filter Control

4.1. Identification of SAPF by P-Q method

This method is based on the $\alpha-\beta$ conversion to remove the real and imaginary powers. Given that (v_α, v_β) and (i_α, i_β) are the orthogonal components of the $\alpha-\beta$ reference associated respectively with the connection voltages of the parallel active filter (v_s) and the currents absorbed by the polluting loads (i_L). In order to calculate the real and imaginary power, this method uses the $\alpha-\beta$ transformation.

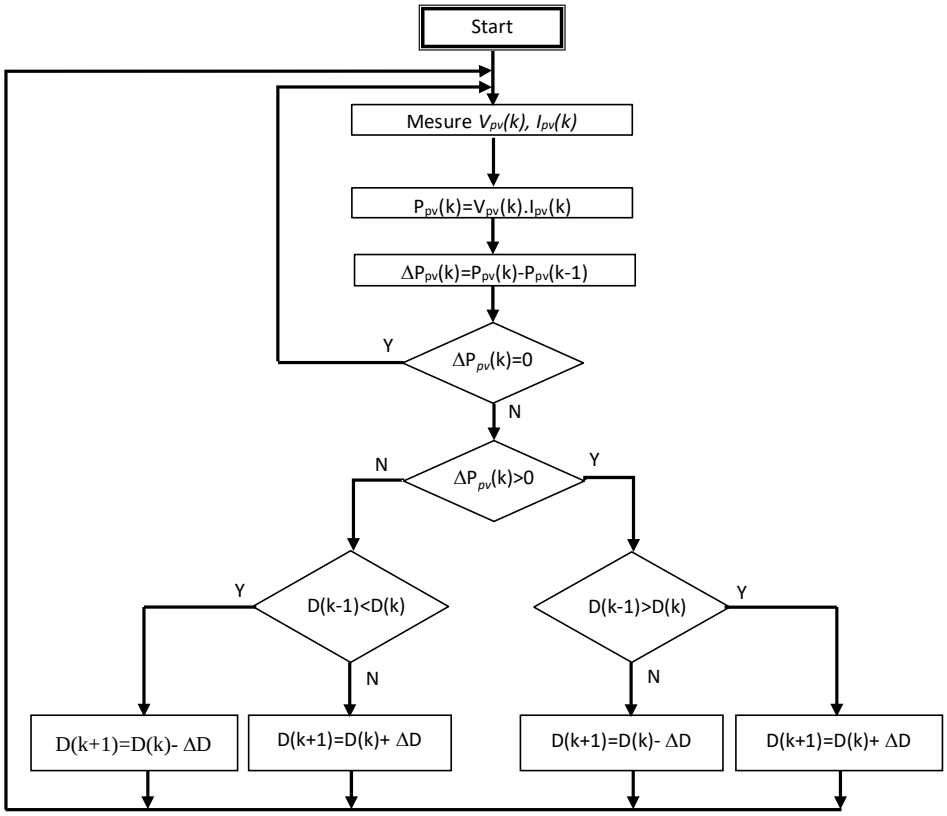

Figure 7. Perturb and Observe (P&O) algorithm

$$[v_s]=\begin{bmatrix} v_{sa} \\ v_{sb} \\ v_{sc} \end{bmatrix} \text{ and } [i_s]=\begin{bmatrix} i_{sa} \\ i_{sb} \\ i_{sc} \end{bmatrix} \qquad (10)$$

The three-phase to two-phase transformation of instantaneous voltages and currents is as follows:

The voltages:

$$\begin{bmatrix} v_{s\alpha} \\ v_{s\beta} \end{bmatrix}=\sqrt{\frac{2}{3}}\cdot\begin{bmatrix} 1 & -\frac{1}{2} & -\frac{1}{2} \\ 0 & \frac{\sqrt{3}}{2} & -\frac{\sqrt{3}}{2} \end{bmatrix}\cdot\begin{bmatrix} v_{sa} \\ v_{sb} \\ v_{sc} \end{bmatrix} \qquad (11)$$

and the currents:

$$\begin{bmatrix} i_{L\alpha} \\ i_{L\beta} \end{bmatrix}=\sqrt{\frac{2}{3}}\cdot\begin{bmatrix} 1 & -\frac{1}{2} & -\frac{1}{2} \\ 0 & \frac{\sqrt{3}}{2} & -\frac{\sqrt{3}}{2} \end{bmatrix}\cdot\begin{bmatrix} i_{La} \\ i_{Lb} \\ i_{Lc} \end{bmatrix} \qquad (12)$$

Expression (13) represents the active and reactive powers:

$$\begin{bmatrix} p \\ q \end{bmatrix}=\begin{bmatrix} v_{s\alpha} & v_{s\beta} \\ -v_{s\beta} & v_{s\alpha} \end{bmatrix}\cdot\begin{bmatrix} i_{L\alpha} \\ i_{L\beta} \end{bmatrix} \qquad (13)$$

If the phase equivalent voltages and currents replace their two-phase equivalents, then:

$$\begin{cases} p = v_{S\alpha} \cdot i_{L\alpha} + v_{S\beta} \cdot i_{L\beta} \\ q = v_{S\alpha} \cdot i_{L\beta} + v_{S\beta} \cdot i_{L\alpha} \end{cases} \quad (14)$$

$$\begin{cases} p = v_{Sa} \cdot i_{La} + v_{Sb} \cdot i_{Lb} + v_{Sc} \cdot i_{Lc} \\ q = \frac{1}{\sqrt{3}}\left[\left(v_{Sa} - v_{Sb}\right) i_{Lc} + \left(v_{Sb} - v_{Sc}\right) i_{La} + \left(v_{Sc} - v_{Sa}\right) i_{Lb} \right] \end{cases} \quad (15)$$

from (13), asking:

$$\Delta = v_{S\alpha}^2 + v_{S\beta}^2 \quad (16)$$

we have:

$$\begin{bmatrix} i_{L\alpha} \\ i_{L\beta} \end{bmatrix} = \frac{1}{\Delta} \left\{ \begin{bmatrix} v_{s\alpha} & -v_{s\beta} \\ v_{s\beta} & v_{s\alpha} \end{bmatrix} \cdot \begin{bmatrix} p \\ q \end{bmatrix} \right\} \quad (17)$$

or,

$$\begin{bmatrix} i_{L\alpha} \\ i_{L\beta} \end{bmatrix} = \frac{1}{\Delta} \left\{ \begin{bmatrix} v_{s\alpha} & -v_{s\beta} \\ v_{s\beta} & v_{s\alpha} \end{bmatrix} \cdot \begin{bmatrix} p \\ 0 \end{bmatrix} + \begin{bmatrix} v_{s\alpha} & -v_{s\beta} \\ v_{s\beta} & v_{s\alpha} \end{bmatrix} \cdot \begin{bmatrix} 0 \\ q \end{bmatrix} \right\}$$

$$= \begin{bmatrix} i_{L\alpha p} \\ i_{L\beta p} \end{bmatrix} + \begin{bmatrix} i_{L\alpha q} \\ i_{L\beta q} \end{bmatrix} \quad (18)$$

with,

$$\begin{cases} i_{F\alpha p} = \dfrac{v_{S\alpha}}{\Delta} \cdot p \\ i_{F\alpha q} = \dfrac{v_{S\beta}}{\Delta} \cdot q \end{cases} \text{ and } \begin{cases} i_{F\beta p} = \dfrac{v_{S\beta}}{\Delta} \cdot p \\ i_{L\beta q} = \dfrac{v_{S\alpha}}{\Delta} \cdot q \end{cases} \quad (19)$$

Along axes α and β, the instantaneous powers are given by:

$$\begin{bmatrix} p_\alpha \\ p_\beta \end{bmatrix} = \begin{bmatrix} v_{S\alpha} & i_{L\alpha} \\ v_{S\beta} & i_{L\beta} \end{bmatrix} = \begin{bmatrix} v_{S\alpha} & i_{L\alpha p} \\ v_{S\beta} & i_{L\beta p} \end{bmatrix} + \begin{bmatrix} v_{S\alpha} & i_{L\alpha q} \\ v_{S\beta} & i_{L\beta q} \end{bmatrix}$$

$$= \begin{bmatrix} p_{\alpha p} \\ p_{\beta p} \end{bmatrix} + \begin{bmatrix} p_{\alpha q} \\ p_{\beta q} \end{bmatrix} \quad (20)$$

$$\begin{cases} p_{\alpha p} = \dfrac{v_{S\alpha}^2}{\Delta} \cdot p \\ p_{\alpha q} = -\dfrac{v_{S\alpha} \cdot v_{S\beta}}{\Delta} \cdot q \end{cases} \text{ and } \begin{cases} p_{\beta p} = \dfrac{v_{S\beta}^2}{\Delta} \cdot p \\ p_{\beta q} = \dfrac{v_{S\alpha} \cdot v_{S\beta}}{\Delta} \cdot q \end{cases} \quad (21)$$

From (15), we can write:

$$p = p_{\alpha p} + p_{\beta p} + p_{\alpha q} + p_{\beta q} = p_{\alpha p} + p_{\beta q} \quad (22)$$

where p and q express the active and reactive powers which are defined by:

$$\begin{cases} p = \bar{p} + \tilde{p} \\ q = \bar{q} + \tilde{q} \end{cases} \quad (23)$$

or, $\bar{p}$ and $\bar{q}$ represent the continuous active and reactive powers related to the fundamental component of the current; $\tilde{p}$ and $\tilde{q}$ represent the alternating active and reactive powers linked to the sum of the harmonic components of the current.

$$\begin{bmatrix} i^*_{Fa} \\ i^*_{Fb} \\ i^*_{Fc} \end{bmatrix} = \sqrt{\frac{2}{3}} \begin{bmatrix} 1 & 0 \\ -\frac{1}{2} & \frac{\sqrt{3}}{2} \\ -\frac{1}{2} & -\frac{\sqrt{3}}{2} \end{bmatrix} \cdot \begin{bmatrix} i^*_{F\alpha} \\ i^*_{F\beta} \end{bmatrix} \quad (24)$$

Figure 8 represents the P-Q method expressing the extraction of harmonic currents [13].

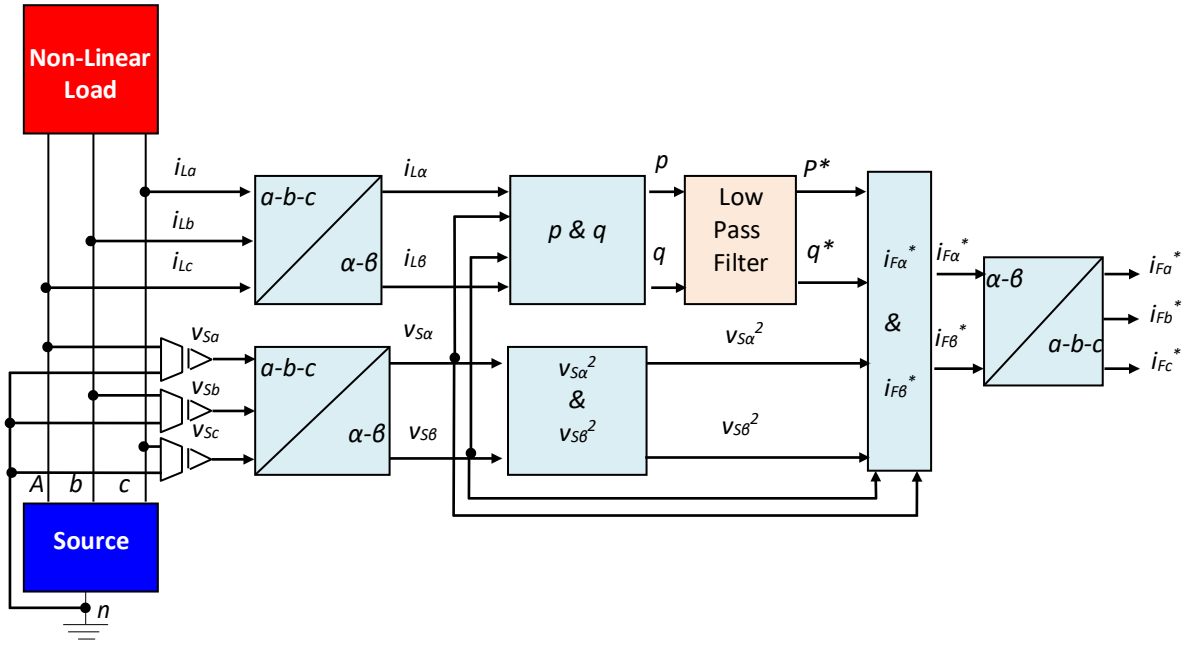

Figure 8. "P-Q" method - Extraction of Harmonic Currents

4.2. Artificial Neural Networks control

ANN is trained by three steps, namely the architecture, the training algorithm and its activation function. The activation functions are ensured only by activation while each neuron is connected to the other. The NNA runs a sentencing standard intended to make the system robust [14].

Figure 9 shows the multilayer perceptron (MLP) which is used for harmonics attenuation and it consists of three inputs as shown in the model of the figure. The rapid estimation of the Fourier coefficients equivalent to the harmonics is an advantage of ANN [15]. The application of data trained by Levenberg Marquardt (LM) helped us to use the Back Propagation (BP) algorithm for the simulation. For layer 1, the transfer function is “logsig”. While For layer 2 or hidden layer, the transfer function is “tansig”. There are 3 neurons in the first layer and 10 neurons in the second layer. For desired optimal results, the output layer depends on the type of data to be analyzed.

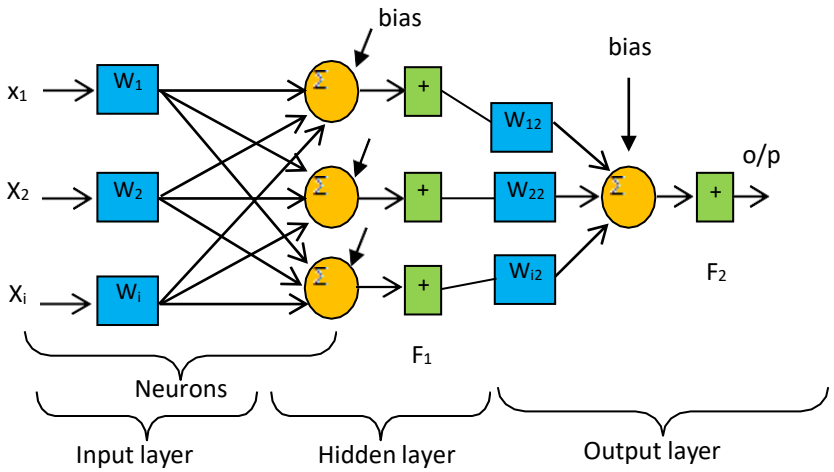

Figure 9. Artificiel Neural Networks structure

5. Simulation Results and Discution

5.1. Simulation Results of PV system

Figures 10 to 13 represent different results of PV system used with parameters shown in Table 1 and number of modules in series 19 and in parallel 10.

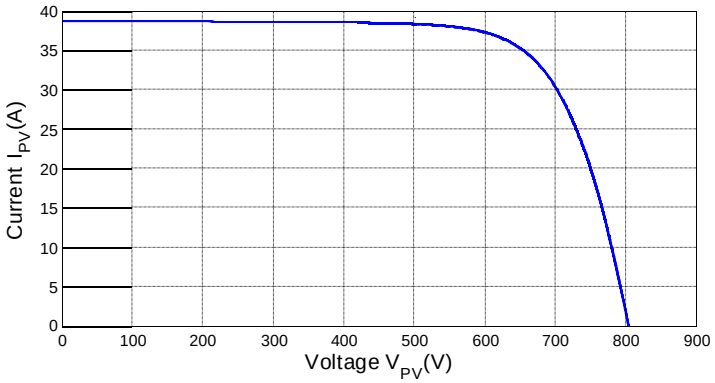

Figure 10. IPV-VPV curve of PV system

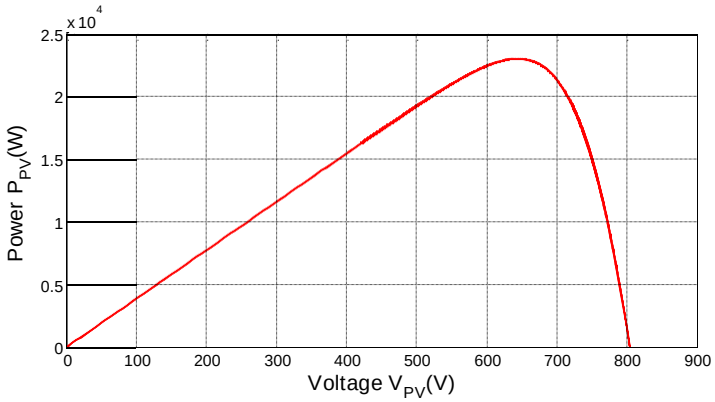

Figure 11. PPV-VPV curve of PV system

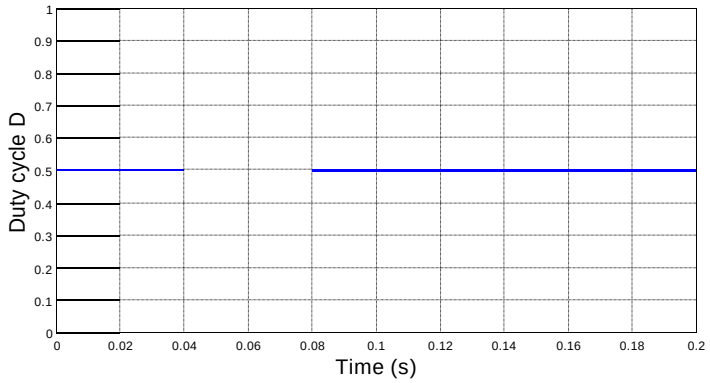

Figure 12. Duty cycle (D)

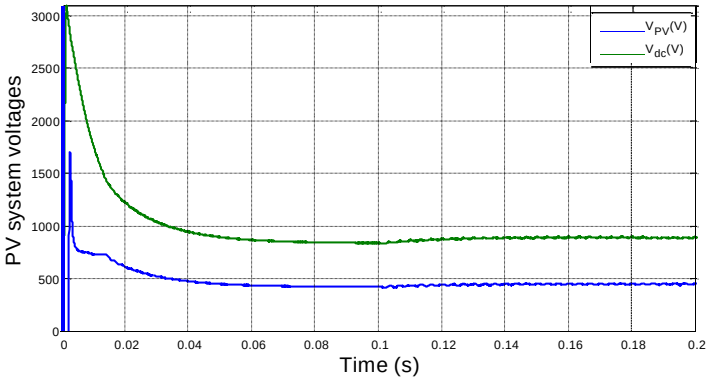

Figure 13. VPV and V_{dc} curves of PV system

5.2. Simulation results of SAPF

In order to model and test the system under the MATLAB/Simulink environment, using the P-Q algorithm method, with PI then ANN controllers. Table 2 shows the parameter values of the system:

Table 2. Simulation parameter values

Parameters	Values
Supply's voltage v_S and frequency f	220Vrms, 50 Hz
Line's inductance L_s and resistance R_s	19.4 µH, 0.25 mΩ
DC link's inductance L_{dc}, resistance R_{dc}	20 mH, 6.5 Ω
Load inductance L_F	1.5 mH
DC link voltage V_{dc}, Coupling inductance L_{Fa}, resistance R_{Fa}	840 V 1.5 mH, 5 mΩ

Figure 14 shows the different simulation results of the shunt Active Power Filter (SAPF) system by applying two control strategies. The first is classical; it is the Proportional-Integral (PI) regulator. The second is modern; it is the regulator by Artificial Neural Networks (ANN). Each is in cascade with the P-Q method. Figure 1 has allowed us to compare the characteristics between the two techniques.

Before starting the discussion of the results obtained, we must note that we did both simulations before and after filtering in the same illustration via a switch that closes at the instant 1 s in a range of 2 s.

First, we presented the three supply voltages $v_{S,abc}$ offset by an angle of 2π/3 and have an

amplitude of $220\sqrt{2}$. The waveforms are sinusoidal as shown in the Figure (1.a).

After, we find that the source current i_{Sa} is improved after shunt active filtering became almost sinusoidal after it was deforming i_{La}. The i_{Sa} waveform in the ANN control is closer to sinusoidal than in PI control. This indicates the effectiveness of artificial intelligence in parallel active filtering.

The Total Harmonic Distortion (THD) is decreased from 20.16 % to 3.12 % for the PI regulator and to 1.19 % for the ANN regulator. The zoom clearly showed us the disappearance of multiple harmonic order of 2 and 3.

We thus note that the phase difference between the supply voltage v_{Sa} and the source current i_{Sa} is better than the phase shift with the load current i_{La}. That is, it gets closer to unity especially with the regulator by neural networks.

Figure (1.f) shows the filter current i_{Fa} and its reference i_{Fa}^{*}. We observe that the current iFa is zero before putting the SAPF in service between 0 and 1 s. After 0.1 s, the current iFa follows well the trajectory of i_{Fa}^{*} especially with neural networks as shown by the zoom between 0.18 s and 0.2 s.

Finally, Figure (1.g) shows the three currents of the shunt active filtering system. We can see that the load current i_{La} corrected by the filter current i_{Fa}, so that the source current i_{Sa} becomes sinusoidal.

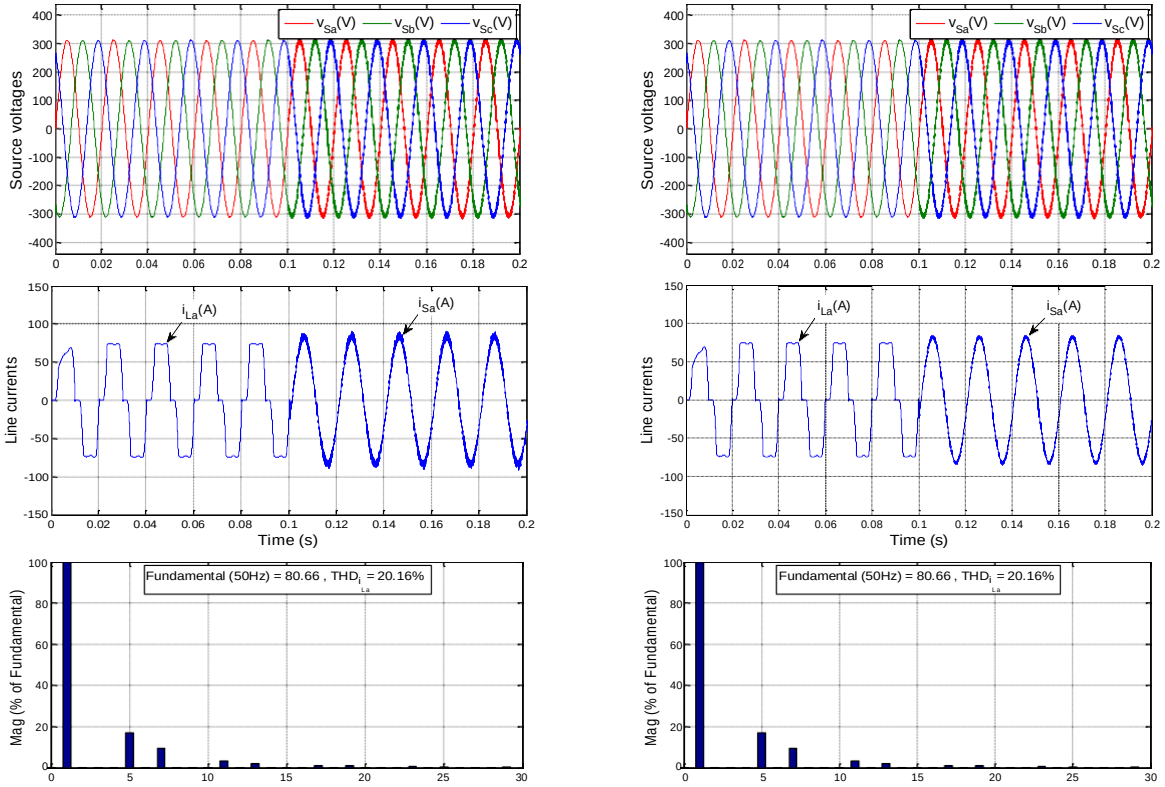

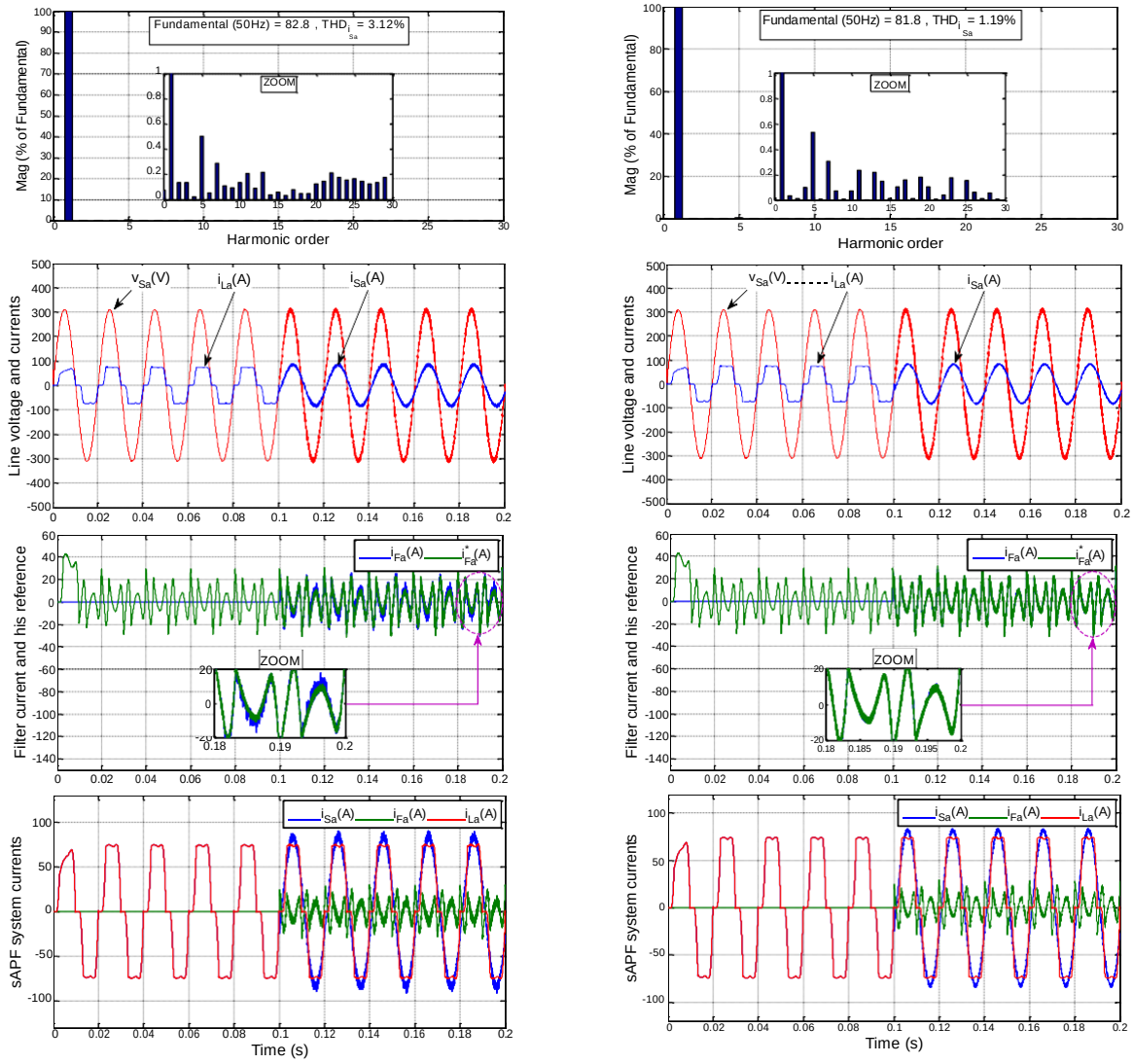

PQ-PI ***PQ-ANN***

Figure 14. Comparison between PQ-PI and PQ-ANN of SAPF powered by a PV system

6. Conclusion

In this paper, we have represented the simulation results of the filter powered by a source of renewable origin (PV) and controlled by the P-Q method in cascade with the PI controller then ANN respectively. The simulation of the shunt active filtering system by supplying the inverter with a photovoltaic source, it has been found that the PV system delivers a stable voltage V_{dc} at the value 840 V since the system has been optimized by the MPPT command with the perturb and observe (P&O) method. Then the $THD_{iLa} = 20.16\%$ decreased to $THD_{iSa}(PI) = 3.12\%$ and $THD_{iSa}(ANN) = 1.19\%$ which is better than the previous regulator. These results are very reasonable and acceptable by the low voltage electrical network according to international recommendations which requires THD less than 5%.

Acknowledgment

Our thanks to all the staff of our LREA research laboratory team at the University of

Medea in Algeria and to Professor Hassan Nouri of the PSECRG Laboratory at the University of West of England, Bristol in the United Kingdom for their useful contributions and their encouragement.

References

[1] M. Popescu, A. Bitoleanu, V. Suru, "Phase Coordinate System and p-q Theory Based Methods in Active Filtering Implementation," Advances in Electrical and Computer Engineering, vol. 13, no. 1, pp. 69-74, 2013. doi:10.4316/AECE.2013.01012

[2] U. Khruathep, S. Premrudeepreechacharn and Y. Kumsuwan, "Implementation of shunt active power filter using source voltage and source current detection," 3rd IEEE Conference on Industrial Electronics and Applications.. pp. 2346–2351, 2008. doi:10.1109/ICIEA.2008.4582937

[3] A. Krama, L. Zellouma, A. Benaissa, B. Rabhi, M. Bouzidi and M. F. Benkhoris, "Design and Experimental Investigation of Predictive Direct Power Control of Three-Phase Shunt Active Filter with Space Vector Modulation using Anti-windup PI Controller Optimized by PSO," Arabian Journal for Science and Engineering, vol. 44, pp. 6741–6755, 2019. doi:10.1007/s13369-018-3611-6

[4] D. Djendaoui, A. Benaissa, B Rabhi and L. Zellouma, "Self Tunning Filter For Three Levels Four Legs Shuntactive Power Filter With Fuzzy Logic Controller," Acta Polytechnica, vol. 61, num.3, pp. 415–427, 2021. doi:10.14311/AP.2021.61.0415

[5] R. Dehini, A. Bassou and B. Ferdi, "The harmonics detection method based on neural network applied to harmonics compensation," International Journal of Engineering, Science and Technology, vol. 2, num. 5, pp. 258-267, 2010. doi:10.4314/ijest.v2i5.60160

[6] R. Bojoi, L. R. Limongi, F. Profumo, D. Roiu and A. Tenconi, "Analysis of Current Controllers for Active Power Filters Using Selective Harmonic Compensation Schemes," IEEJ Transactions on Electrical and Electronic Engineering. vol. 4, num. 2, pp. 139–157, 2009. doi:10.1002/tee.20392

[7] H. AKAGI, "Trends in active power line conditioners," IEEE Transactions on Power Electronics; vol. 9, num. 3, pp. 263–268, 1994. doi:10.1109/63.311258

[8] A. Morsli, A. Tlemçani, A. Moualdia, L. Zellouma, M. S. Boucherit and N. Henini, "Experimental Validation of a Shunt Active Power Filtering System for Improvement the Energy Quality employing the Direct Power Control," 2018 International Conference on Applied Smart Systems (ICASS'2018). 24-25 November 2018, Medea university, Algeria. IEEE Xplore, 2019. doi:10.1109/ICASS.2018.8652074

[9] A. Morsli, A. Tlemçani, N. Ould Cherchali and M. S. Boucherit, "Comparison between PI and fuzzy logic type-1 controllers for improvement the power quality by a shunt active power filter five-level NPC topology," 8th International Conference on Modelling, Identification and

Control (ICMIC-2016) Algiers, Algeria-November 15-17, IEEE Xplore, pp. 243-248, 2016. doi:10.1109/ICMIC.2016.7804116

[10] R. Belaidia, A. Haddouche and H. Guendouz, "Fuzzy Logic Controller Based Three-Phase Shunt Active Power Filter for Compensating Harmonics and Reactive Power under Unbalanced Mains Voltages," Elsevier Energy Procedia vol. 18, pp.560-570, 2012. doi:10.1016/j.egypro.2012.05.068

[11] L. F. C. Monteiro, C. M. Freitas and M. D. Bellar, "Improvements on the Incremental Conductance MPPT Method Applied to a PV String with Single-Phase to Three-Phase Converter for Rural Grid Applications," Advances in Electrical and Computer Engineering, vol. 19, num. 1, pp. 63–70. 2019. doi:10.4316/AECE.2019.01009

[12] A. Bouraiou, M. Hamouda, A. Chaker, M. Sadok, M. Mostefaoui and S. LACHTAR, "Modeling and Simulation of Photovoltaic Module and Array based on One and Two Diode Model Using Matlab/Simulink," International Conference on Technologies and Materials for Renewable Energy, Environment and Sustainability, TMREES15. Energy Procedia vol. 74, pp. 864 – 877, 2015. doi:0.1016/j.egypro.2015.07.822

[13] S. Devassy and B. Singh, "Modified pq-theory-based control of solar-PV-integrated UPQC-S," IEEE Transactions on Industry Applications, vol. 53, no. 5, pp. 5031–5040, 2017. doi:10.1109/TIA.2017.2714138

[14] M. Merah, A. Ouamri, A. Naït-Ali and M. Keche, "Fault Tolerant Neural Network for ECG Signal Classification Systems," Advances in Electrical and Computer Engineering, vol. 11, num. 3, pp. 17–24, 2011. doi:10.4316/AECE.2011.03003

[15] A. Sulehri, M. N. Jeelani and A. A. Ikram, "Power quality improvement in an AC network using artifcial neural network and hysteresis band current controller," IngenIería e InvestIgacIón, vol. 38 num. 3, pp. 42-49, 2018. doi:10.15446/ing.investig.v38n3.67885